Journal of Magnetic Resonance 195 (2008) 123–128

Contents lists available at ScienceDirect

Journal of Magnetic Resonance

journal homepage: www.elsevier.com/locate/jmr

Effective and accurate single-shot NMR diffusion experiments based on magnetization grating

Kosma Szutkowski, István Furó *

Division of Physical Chemistry, Department of Chemistry, Royal Institute of Technology, Teknikringen 30/36, SE-10044 Stockholm, Sweden

ARTICLE INFO

Article history:
Received 5 June 2008
Revised 13 August 2008
Available online 28 August 2008

Keywords:
Diffusion
Single scan
Magnetization grating
DANTE

ABSTRACT

Current single-shot diffusion methods based on magnetization gratings suffer from low sensitivity due to small rf tip angles and, consequently, from inefficient use of the total equilibrium magnetization. Here, we propose and illustrate the use of a slightly modified form of the magnetization encoding scheme OUFIS for single-shot diffusion experiments. In a detailed theoretical and experimental analysis, we compare the performance of the proposed method to other encoding schemes such as the one-phase or two-phase DANTE and conclude that the OUFIS-based experiment is a superior one. The primary reason is that this scheme allows one to use a larger total pulse area. Hence, one can encode a far larger portion of the initial magnetization into a frequency grating before the onset of various nonlinear effects. In the experimental illustration, we present a single-shot measurement of multicomponent diffusion.

1. Introduction

Currently available methods for rapid measurement of diffusion by NMR [1–5] all exploit multiple encoding in *k*-space. Portions of the initial longitudinal magnetization are then subject to distinct encoding and, consequently, to distinct attenuation. Subsequently, one may estimate the diffusion coefficient from the resulting sequence of attenuations. Besides this common element, there are vast differences between the suggested experiments both as concerning efficiency, accuracy, and ease of use. In the ultimate single-shot limit, one exploits the state of thermal equilibrium just once. In practice, not all methods that are claimed to be "single-shot" can reach this limit.

The MMME technique based on multiple modulation and multiple echoes [3] is, in principle, a single-shot method that is very efficient as concerning the number of radiofrequency (rf) pulses used. For example, it excites 13 different coherence transfer pathways if four pulses are applied. However, all excited echoes have different shapes and amplitudes which provides an outcome that is inconvenient to handle. For example, it is unfeasible to have equal magnitude for all observed echoes and therefore one must resort to acquiring additional reference scans. Furthermore, if one wants to use the MMME pulse sequence with more than four pulses, the encoding time expands considerably which results in an increased influence of spin relaxation. MMME in a single scan does not sample the *k*-space in a homogeneous way and therefore the method is less practical for detecting multicomponent diffusional decays. Finally, diffusion time is not strictly defined in MMME which limits its application to restricted diffusion. Despite all those limitations MMME makes use almost as much of the total initial magnetization as does a spin-echo experiment [6] which makes this method a sensitive one [3].

Though not a true single-shot method (since it is based on varying the observation time Δ over which both self-diffusion and relaxation affect the signal and requires therefore reference scans) Difftrain [4,7] is a fast diffusion method of special interest since it maintains chemical shift information. Difftrain is especially useful if multiple diffusion propagators are to be studied [7] in which case it may be one order of magnitude faster than equivalent conventional PGSE experiments. A detailed analysis of the available sequences is provided by Pages and Kuchel [5].

In this paper, we analyze, compare, and demonstrate pulse sequences based on multi-frequency magnetization gratings generated by pulse trains akin to DANTE and applied in the presence of a magnetic field gradient. Though the DANTE pulse train has originally been invented for the purpose of selective excitation [8,9] it was subsequently discovered that, in combination with a magnetic field gradient, it can excite multiple trajectories in the *k*-space [10,11]. Hence, multiple gradient echoes can be created and used in single-shot experiments which can be exploited for fast NMR imaging [10,12]. In particular, the DUFIS experiment (DANTE Ultrafast Imaging Sequence [2]) was adapted by Doran and Décorps [1] and later by Peled et al. [13] for rapidly measuring self-diffusion and flow. The procedure is potentially fast and simple since diffusion coefficients could, in the case of a small tip angle and sufficient signal strength, be derived directly from the gradient

* Corresponding author. Fax: +46 8 790 82 07.
E-mail address: ifuro@physchem.kth.se (I. Furó).

1090-7807/$ - see front matter © 2008 Elsevier Inc. All rights reserved.
doi:10.1016/j.jmr.2008.08.009

echo amplitudes. In practice, diffusion and flow were quantified in sub-second speed.

There are some limitations however. First, no spectral resolution is retained. Secondly, the sensitivity is much lower than that in a spin-echo PGSE experiment [6]. For example, it has been estimated that the DUFIS experiment makes use of significantly less than 20% of the thermal equilibrium magnetization [3]. The total pulse area, the sum of areas of all rf pulses during the excitation period, in a DUFIS experiment must be kept low (far below 90°) or else echo shapes get distorted and echo amplitudes become uneven [3,13].

Notably, Zha and Lowe developed another grating protocol and designed thereby a fast imaging method (OUFIS) that dramatically increased the proportion of total magnetization exploited for grating [14]. As we are going to demonstrate, this particular pulse sequence provides superior performance in single-shot diffusion experiments. The primary reason for this gain is that in the OUFIS experiment most of the sample experiences a relatively small perturbation, while the simple DANTE sequence has a sparse excitation spectrum and hence uses up most of the available magnetization at certain spatial regions. We focus on sensitivity, the linear response of gradient echoes, and the maximum total pulse area during encoding. As we are going to show below, this approach allows one to characterize and quantify diffusion in sufficient detail even in the true single-shot limit.

2. Theory

The generic grating-based diffusion pulse sequence is shown in Fig. 1. The first part is responsible for encoding a magnetization grating in the spatial (that is, frequency) domain. In the second part, the grating is detected as multiple echoes in the time domain; each echo arises as the Fourier transform of a particular sinusoidal component in the prepared magnetization grating. Since Fourier transformation is a linear operation, the amplitude of each echo is proportional to the amplitude of the corresponding component of the grating. If there is a period inserted between encoding and detection, diffusion of the molecules during that period decreases the amplitude of the grating component which is detected as a decrease of the amplitude of the corresponding echo.

2.1. DANTE-based grating encoding schemes

The encoding sequence of the single-phase DANTE scheme [8,9] is

$$[\alpha_x - \tau -]_n, \tag{1}$$

where α_x is an rf pulse of tip angle α applied along the x axis in the rotating frame, τ is the time interval between pulses and n is the number of repetitions. If applied in the pulse sequence in Fig. 1 and in the presence of a constant magnetic field gradient along the direction z, one obtains a complex multiple modulation the longitudinal magnetization [11]. In the small tip angle limit $\sin(\alpha) = \alpha$ this modulation simplifies to

$$M_{\mathrm{long}}(z) = \alpha \sum_{k=1}^{n} \cos[\gamma g z (d_m + k\tau)], \tag{2}$$

where g is the gradient strength and γ is the magnetogyric ratio, and the equilibrium magnetization is set to unity. Destructive interference among the inscribed cosines leads to a comb-like spatial (that is, frequency) distribution of magnetization; it is this comb-like distribution that is also exploited for the purpose of selective excitation in spectroscopic applications. As discussed below, the same interference does not allow this sequence to make efficient use of the available magnetization in imaging or diffusion experiments.

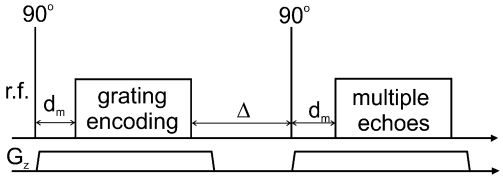

Fig. 1. The generic grating-based diffusion pulse sequence. The grating encoding block consists of rf pulses with small tip angles separated by appropriate delays. The created magnetization grating is a linear combination of sinusoidal patterns of longitudinal magnetization. During period Δ those patterns decay as a result of diffusion. The remaining pattern is detected as an echo signal.

The magnetization grating encoded by the DANTE pulse sequence is utilized in DUFIS and BURST type pulse sequences [1,2,13]. As is well known [15], if one encodes periodic patterns of molecular properties (nuclear magnetization patterns by NMR or patterns of optical properties as in, e.g., FRET) the amplitudes of patterns decay as an effect of the diffusion and the rate of decay depends on the periodicity of the pattern [15]. In Fig. 1, this decay takes place during the period Δ. The amplitudes of the individual sinusoidal components are then detected during the second half of the pulse sequence; the second 90° pulse turns the longitudinal magnetization grating into a transverse one and the different sinusoidal components of transverse magnetization are detected in time domain as sharp echoes. The Fourier relation between the frequency domain (sinusoidal patterns) and time domain (echoes) associates the echo placement with the corresponding encoded frequencies.

The diffusion coefficient D is obtained by fitting the calculated function of attenuation to the obtained series of echo intensities [13]. In our present case and under the assumption of negligible gradient switching time after the first rf pulse in the sequence, the attenuation function becomes (with periods as given in Fig. 1 and Eq. (1)) for the nth echo

$$A_n = \exp\left\{-D(\gamma g)^2 [d_m + (n-1)\tau]^2 \left(\Delta + \frac{2}{3}[d_m + (n-1)\tau]\right)\right\}, \tag{3}$$

where $\Delta + \frac{2}{3}[d_m + (n-1)\tau]$ is the diffusion time for the respective echo. Concerning practical aspects, the experiment could also be performed using a constant magnetic field gradient; however, the 90° rf pulses must then be short enough to provide excitation over a wide enough frequency range. As compared to previous implementations [13], the pulse sequence in Fig. 1 also uses delay d_m in order to provide a clear separation between desired echo signals and the artifact from the transient created by the second 90° pulse. As another difference, the present pulse sequence uses DANTE-type excitation to produce longitudinal magnetization from the transverse magnetization prepared by the initial 90° pulse. In previous implementations, this was done in reverse order [13].

An improvement to the DANTE method is based on cycling the phase of the excitation pulses [12]. Hence, alternating the phase between 0° and 90°, that is

$$[\alpha_x - \tau - \alpha_y - \tau -]_n, \tag{4}$$

doubles the number of tags in the comb with an alternating cosine–sine grating with the same frequencies as in Eq. (2). In the time domain, we have a corresponding phase modulation of the echoes.

It was also found, but not explained in detail, that this latter experiments allows one to increase the tip angles and thereby the signal-to-noise ratio [2] while keeping the magnetization approximately as expressed in Eq. (2). With encoding as in Eq. (4), the phase of the first 90° pulse can be set halfway between x and y which yields homogeneous echo amplitudes.

2.2. OUFIS encoding

Since phase alternation as above improves the performance of DANTE-type excitations, the question arises as to which excitation sequence, consisting of small tip angle pulses of different phases, provides the most efficient use of the available magnetization. This question was answered by means of computer optimization [14] which yielded several options of pulse trains collectively termed as OUFIS sequences. One of the simplest yet efficient pulse sequence consists of 16 low tip angle pulses

$$[\alpha_x-\tau-(\alpha_{-x}-\tau)_4-(\alpha_x-\tau)_4-\alpha_{-x}-\tau-(\alpha_x-\tau)_3-\alpha_{-x}-\tau-(\alpha_x)_2-\tau-]_n. \quad (5)$$

As we are going to illustrate below the spatial distribution of magnetization becomes, instead of that described by Eq. (2), a linear combination of sine and cosine terms. This linear combination is such that the frequency spectrum of excitation is no longer comb-like. On the other hand, the different harmonic terms will suffer less destructive interference which results in more initial magnetization encoded as harmonic patterns. Below we are going to investigate this pulse sequence concerning its application in single-shot diffusion experiments and compare its performance there to the more conventional DANTE-type excitations.

3. Calculating magnetization gratings

3.1. Calculation methods

Outside the small tip angle limit, the generated magnetization grating deviates from the one given in Eq. (2). First, the grating intensities A_n become unequal to each other and, secondly, the modulation ceases to be pure cosine. Qualitatively, this situation arises because at certain spatial regions (for DANTE, the regions of selective excitation) the pulse sequence in Fig. 1 uses up all available longitudinal magnetization. Operationally, one can define the small angle limit by identical grating intensities A_n. Since the pulse sequences introduced above are different as concerning their excitation frequency profile, they also differ from each other in regards to the total pulse area achieved when they reach their respective small tip angle limit. As concerning diffusion experiments, this is important not least because single-shot experiments (that is, without reference experiments) require identical A_n values so that from the detected echo intensities one obtains the true attenuation series as provided by Eq. (3).

To calculate the magnetization gratings generated by the different pulse sequences, we use a simple vector model and transformations based on rotation matrices [16]. The simulated magnetization profile consists of five thousand unit magnetization vectors that are uniformly distributed along direction z in space. Those magnetization vectors correspond to thin slices of the investigated sample, each of which possesses its characteristic resonance frequency $\omega(z) = \gamma g_z z$. The effect of rf pulses and free evolution is represented by 3×3 rotation matrices $\mathbf{R}_{x,y,z}(\alpha)$

$$\mathbf{R}_x(\alpha) = \begin{bmatrix} 1 & 0 & 0 \\ 0 & \cos(\alpha) & \sin(\alpha) \\ 0 & -\sin(\alpha) & \cos(\alpha) \end{bmatrix},$$
$$\mathbf{R}_y(\alpha) = \begin{bmatrix} \cos(\alpha) & 0 & -\sin(\alpha) \\ 0 & 1 & 0 \\ \sin(\alpha) & 0 & \cos(\alpha) \end{bmatrix}, \quad (6)$$
$$\mathbf{R}_z(\alpha) = \begin{bmatrix} \cos(\alpha) & \sin(\alpha) & 0 \\ -\sin(\alpha) & \cos(\alpha) & 0 \\ 0 & 0 & 1 \end{bmatrix}.$$

The effect of an rf pulse α_φ is simply calculated by rotating the magnetization prior to the pulse

$$\mathbf{M}_-(z) = \begin{bmatrix} M_x(z) \\ M_y(z) \\ M_z(z) \end{bmatrix}, \quad (7)$$

as

$$\mathbf{M}_+(z) = \mathbf{R}_x(\alpha) \cdot \mathbf{R}_z(\varphi) \cdot \mathbf{M}_-(z). \quad (8)$$

In other words, rf excitation is assumed to be spatially homogeneous. On the other hand, the effect of evolution in a magnetic field gradient g_z is described by the rotation matrix

$$\mathbf{G}_z(z,\tau) \equiv \mathbf{R}_z(\omega_z \cdot \tau). \quad (9)$$

In this representation, the effect of, e.g., the DANTE scheme in Eq. (1) embedded in the pulse sequence in Fig. 1, is described as

$$\mathbf{M}^{xx}(z)_n = [\mathbf{G}_z(z,\tau) \cdot \mathbf{R}_x(\alpha)]_n \cdot \mathbf{G}_z(z,d_m) \cdot \mathbf{R}_x(90^\circ) \cdot \mathbf{R}_z(\varphi) \cdot \mathbf{M}_0(z), \quad (10)$$

where ϕ is the phase to the first rf pulse and

$$\mathbf{M}_0(z) = \begin{bmatrix} 0 \\ 0 \\ 1 \end{bmatrix} \quad (11)$$

is the equilibrium magnetization vector at position z. Similarly, the effect of pulse sequence in Eq. (4) can be represented as

$$\mathbf{M}^{xy}(z)_n = [\mathbf{G}_z(z,\tau) \cdot \mathbf{R}_y(\alpha) \cdot \mathbf{G}_z(z,\tau) \cdot \mathbf{R}_x(\alpha)]_n \cdot \mathbf{G}_z(z,d_m) \cdot \mathbf{R}_x(90^\circ) \cdot \mathbf{R}_z(\varphi) \cdot \mathbf{M}_0(z). \quad (12)$$

Analogous expressions can be easily derived for the two-phase OUFIS modulation.

For each investigated pulse sequence, the generated profile of longitudinal magnetization $M_z(z)$ at the grating encoding block is created by projecting the magnetization vector at the end of the pulse train onto the z axis. Experimentally, $M_z(z)$ is retained and transverse components are suppressed by a spoiling gradient pulses. For our purpose, see below, it sufficed to compare the simulated and experimental magnetization gratings at the shortest possible diffusion times and therefore it was not necessary to include explicit relaxation and diffusion effects in our calculations. The final result is the longitudinal magnetization versus position z, $M_z(z)$, and its Fourier transform; the experimental quantity that corresponds to the latter, disregarding a constant scaling, is the magnitude of the transverse magnetization $\sqrt{M_x^2 + M_y^2}$ over the echo train obtained in the time domain. The actual calculations were performed using Mathcad 13 software with parameters as follows: the number of low tip angle encoding pulses was 16, the time between those pulses—that is, the gradient duration—was set to $\tau = 100$ μs, gradient amplitude was $g = 0.074$ T/m.

If necessary, one might easily include diffusion and relaxation effects. Spin relaxation can simply be accounted for by scaling down all the amplitudes in-between rf pulses by the assumed relaxation rates. Diffusion effects can, on the other hand, be easily implemented by a finer mesh and by randomly, using Gaussian statistics, shifting the magnetization vectors to new positions.

3.2. Calculation results and discussion

Gratings of longitudinal magnetization $M_z(z)$ and their corresponding magnitude spectra calculated for one-phase DANTE, two-phase DANTE and two-phase OUFIS modulations, in all cases with the total pulse area corresponding to 20°, are shown in Fig. 2. The same type of results, but for a larger total pulse area of 90°, are shown in Fig. 3. Recall that the spectra represent the

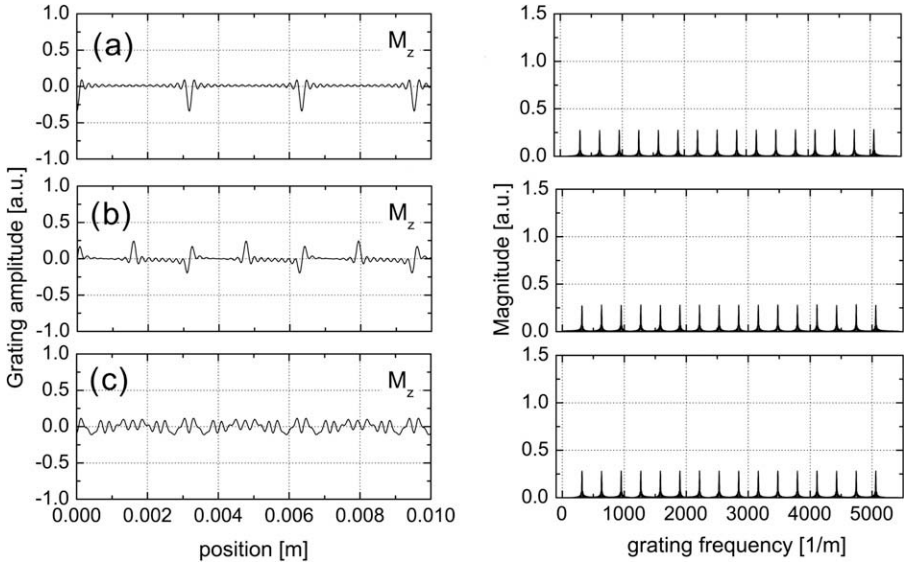

Fig. 2. Calculated magnetization gratings (left) and corresponding magnitude spectra (right) for the total pulse area 20° with 16-pulse encoding sequences (a) one-phase DANTE, (b) two-phase DANTE and (c) two-phase OUFIS, in all cases with setting $d_m = \tau$.

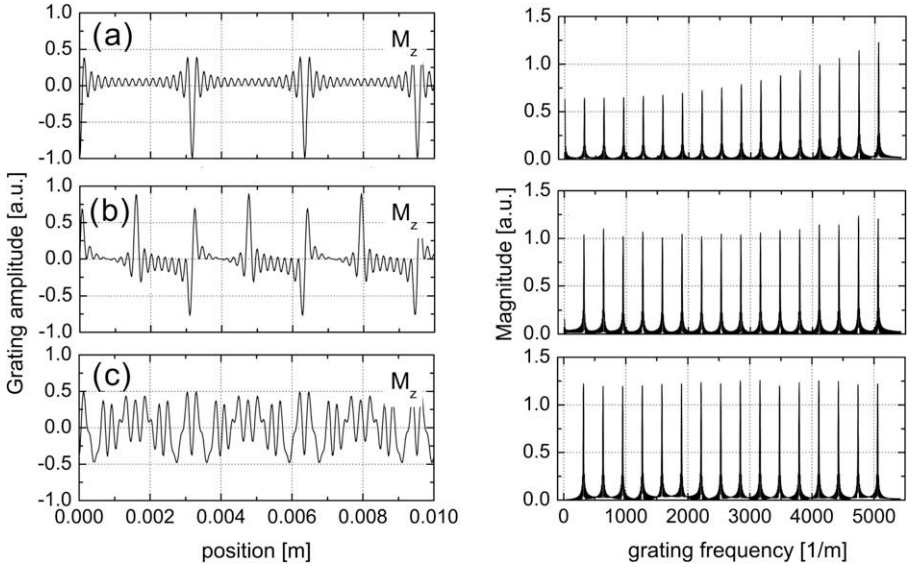

Fig. 3. Calculated magnetization gratings (left) and corresponding magnitude spectra (right) for the total pulse area 90° with 16-pulse encoding sequences (a) one-phase DANTE, (b) two-phase DANTE and (c) two-phase OUFIS, in all cases with setting $d_m = \tau$.

detected time-domain echo trains. As shown by Fig. 2, the envelope of spectral magnitudes and, therefore, the envelope of the detected echoes is uniform at a small total pulse area (20°). In other words, we are in the small tip angle limit as described by Eq. (2). In this limit, the different pulse sequences perform equally well. On the other hand, a small total pulse area provides small signal-to-noise ratio and therefore one wishes to see how well the methods perform at larger total pulse areas.

There, the situation is very different (Fig. 3) and we clearly deviate from the small tip angle regime. The envelope of spectral magnitudes becomes very uneven for the one-phase DANTE (Fig. 3a). This is a consequence of saturation that arises from the coherent addition of cosine gratings with frequencies ω, 2ω, 3ω, ... at certain points in space. In contrast to the one-phase DANTE, the type of modulation in two-phase DANTE changes from pure cosine to cosine–sine. Hence, at the same total pulse area one uses up less of the available magnetization at the most affected regions and, therefore, the onset of saturation is shifted to larger total pulse areas. As shown by Fig. 3c, this effect is even more pronounced for the two-phase OUFIS—there are no sharp peaks, opposite to that in Fig. 3a, in the spatial distribution of the grating amplitude.

One way to illustrate the emergence of nonlinear behavior of the magnetization grating is by plotting the maximum grating amplitude for different modulation types as a function of the total pulse area. This is shown with Fig. 4a. The initial variation of the maximum grating amplitude is roughly sinusoidal but with different periods for each grating scheme. Nonlinearity of the spectral magnitudes sets in where those sinusoidal functions start to significantly deviate from linear ones; qualitatively, this behavior arises because any additional encoding pulse (after the ones that amount to the presented total pulse area) can provide less and less encoded magnetization.

To provide a rough measure of the available range of total pulse area, we show in Fig. 4a the total pulse areas where the maximum

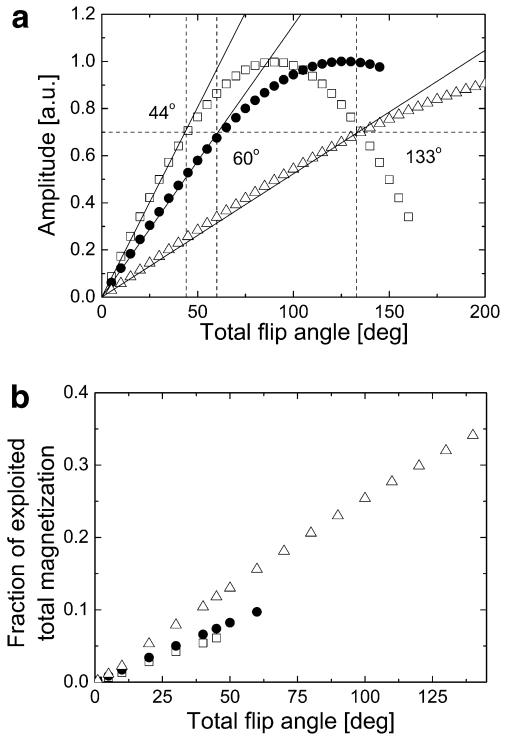

Fig. 4. The maximum grating amplitude (a) and fraction of total magnetization exploited in the different pulse sequences (b) as the function of the total pulse area, calculated for one-phase DANTE (open squares), two-phase DANTE (close circles) and two-phase OUFIS pulses (open triangles) encoding sequences. In all cases, 16 pulses were used and $d_m = \tau$ was set.

exploited magnetization at any spatial point reaches 0.7; there, the sine function deviate from the linear one by ca. 8%. In other words, at the indicated total pulse areas we expect that the respective pulse sequence produces a few percent variation along the detected echo amplitudes. Clearly, the OUFIS encoding allows for much higher total pulse areas while maintaining a uniform envelope of the magnitude spectrum (that is, magnitudes of echoes). Higher total pulse area leads to that a larger portion of the initially available longitudinal magnetization being encoded as grating. This latter point is illustrated in Fig. 4b. Hence, we expect that OUFIS encoding allows one to perform grating-based single-scan diffusion experiments with a signal-to-noise ratio that is far higher than those available by the other DANTE-based schemes. This point is further illustrated below by experiments.

An artifact that becomes accentuated at high total pulse areas is that the pulses in the encoding train create not only a longitudinal grating but, to a smaller extent, also refocus the evolution of the transverse magnetization (also described as confounding pathways [11]). This effect can be visualized best at large d_m values where the ideal experiment is expected to create echoes at times $>d_m$ after the last 90° pulse (see Fig. 1). Partial refocusing leads to magnetization components that are phase-modulated by less than $\gamma g z d_m$ and, hence, yields echoes at times $<d_m$. As one practical aspect, OUFIS encoding yields much smaller refocusing effects than one- or two-phase DANTE. One can also note that at small d_m the secondary echoes produced by partial refocusing are overlapping with the primary echoes. In practice, this latter effect is less important since at the total pulse area where the secondary echoes start to become significant the echo envelope is already nonuniform.

4. Experimental: results and discussion

The experiments were performed on a Bruker AVANCE II DRU spectrometer (300 MHz) equipped with a Micro2.5 microimaging probe with maximum "XYZ" gradients of 1.5 T/m and with a 10-mm rf insert which provided a 90° pulse length of 12.5 μs. We used throughout a dwell time of 2 μs. The digitally filtered time domain data were transformed to accurate time series by the "convdta" routine. Experimental verification and calibration was performed with a 10% H_2O in D_2O sample, put into a 5-mm sample tube up to a height of ca. 15 mm. The experimental scheme was as provided in Fig. 1 with one exception: the gradient was switched on before the second 90° pulse. This has reduced some gradient-switching transients which otherwise distorted somewhat the echoes. In the diffusion experiment below (see Fig. 6) this resulted in the second 90° pulse not providing a nonselective excitation over the spatial distribution of magnetization. However, in the time domain, the sole effect of this is a uniform decrease of the echo magnitudes but no change in the shape of the echo envelope.

The magnetization gratings obtained by one-phase DANTE, two-phase DANTE and two-phase OUFIS encodings for short diffusion times set with $\Delta = 3$ ms (see Fig. 1) and with different total pulse areas are shown in Fig. 5. The findings confirm the results of calculations for all encoding sequences. The one-phase DANTE pulse sequence gives linear response at small tip angles but it significantly deviates from linearity at 69° total pulse area. The shape of envelope of the spectral magnitudes is also in good agreement with calculations: lower frequencies are damped first. Two-phase DANTE performs better but is clearly failing at 92° total pulse area. In contrast to those sequences, the two-phase OUFIS encoding provides a linear response and, therefore, a reasonably uniform envelope of spectral magnitudes even at 115° the total pulse area.

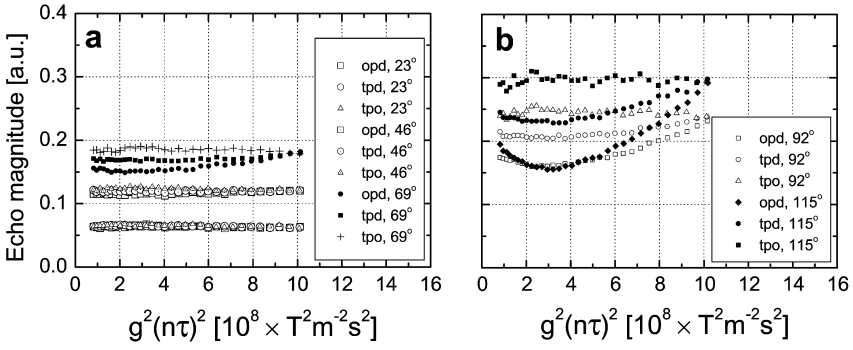

Fig. 5. The comparison of experimental echo magnitudes for selected total pulse area and short $\Delta = 3$ ms. Abbreviations used: "opd", one-phase DANTE; "tpd", two-phase DANTE; "tpo", two-phase OUFIS. All data are single-scan, recorded with an encoding/reading gradient of $g = 0.073$ T/m, and with pulse separations $\tau = 0.1$ ms and $d_m = 1$ ms, see Fig. 1.

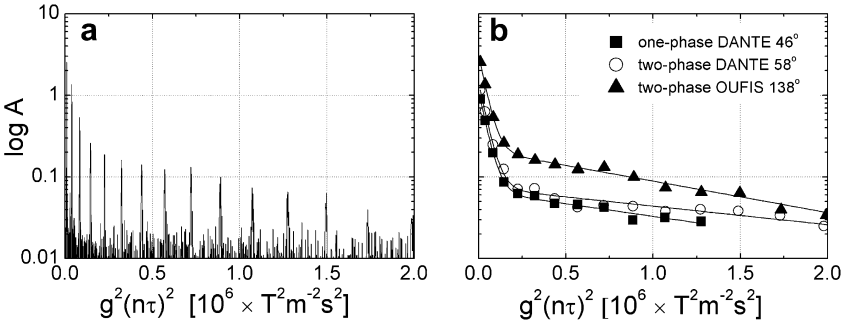

Fig. 6. (a) The signal magnitude of the time-domain echo train detected in a single-scan diffusion experiment performed by the two-phase OUFIS encoding, with the total pulse area of 138°, diffusion time $\Delta = 200$ ms and gradient strength $g = 0.372$ T/m. (b) A comparison between one-phase DANTE, two-phase DANTE and two-phase OUFIS single-scan diffusion experiments performed close to the end of their region of applicability; solid lines represent fits by the sum of two terms given in Eq. (3) but with different diffusion coefficients. Echoes falling below the noise level were omitted. The results of the fits are given in Table 1.

Table 1
Estimated diffusion coefficients and their relative weights representative for water and PEG ($M_w = 6000$) as obtained in their mixture (see text) by a conventional PGSE experiment and by single-scan diffusion experiments using one- and two-phase DANTE and two-phase OUFIS encodings

	I_{H_2O}	D_{H_2O} (10^{-9} m^2 s^{-1})	I_{PEG}	D_{PEG} (10^{-11} m^2 s^{-1})
Conventional PGSE	0.91	1.64	0.09	5.7
One-phase DANTE	0.94	1.73	0.06	4.9
Two-phase DANTE	0.95	1.70	0.05	3.6
Two-phase OUFIS	0.93	1.82	0.07	6.1

To demonstrate the performance of the different pulse sequences, a single-scan diffusion experiment was performed in a sample that consisted of polyethylene glycol (PEG), $M_w = 6000$, from Fluka dissolved at 3 wt% in a 1:3 mixture of H_2O in D_2O (yielding a ratio of H_2O/PEG protons of around 9.8). Because of the large size difference between PEG and water, one expects a two-component decay of the signal. Hence, the obtained echo train magnitudes (see Fig. 6) were fitted by a sum of two terms like that in Eq. (3) but with different diffusion coefficients. The results of this two-component analysis are presented in Table 1 and compared to the values obtained by a conventional PGSE experiment (where the signal-to-noise ratio at one scan at the lowest gradient was 1.7×10^4 in the frequency domain). Clearly, the two-phase OUFIS experiment gives better overall estimates of the relative intensities of the components and their self-diffusion coefficients. This is to a large extent a consequence of the much higher available signal; for the one- and two-phase DANTE modulations, the signal is hardly out of the noise. Note that the observed ca. 10% discrepancy between the diffusion coefficients of the water component obtained by the different methods arises largely because of the small number [3,4] of data points that are sensitive to that parameter.

5. Conclusions

In NMR, the application range of single-scan experiments is often limited by the available signal-to-noise ratio. Hence, experimental modifications that extract the desired information from a higher signal are in constant demand. Above we demonstrated that the encoding scheme OUFIS, previously introduced for fast MRI [14], provides superior performance when compared to other, more usual encoding schemes employed in single-scan diffusion experiments based on magnetization gratings. The superior performance arises from a more efficient use of the available magnetization. We quantify this latter point and demonstrate, both by calculations and by experiments, the range of experimental parameters within which this experiment performs well. As we also show, the signal-to-noise ratio is, indeed, sufficient to characterize a two-component diffusion process by a single-scan experiment (apparently, this has not been done previously [5]). The good performance of the single-scan OUFIS-based diffusion experiment can be advantageous when, among others, attempting diffusion studies with laser-polarized gas [13] or in nonequilibrium systems [17,18].

Acknowledgments

This work has been supported by the Knut and Alice Wallenberg Foundation and the Swedish Research Council VR.

References

[1] S.J. Doran, M. Decorps, A robust single-shot method for measuring diffusion coefficients using the "Burst" sequence, J. Magn. Reson. A 117 (1995) 311–316.
[2] I.J. Lowe, R.E. Wysong, Dante Ultrafast Imaging Sequence (Dufis), J. Magn. Reson. B 101 (1993) 106–109.
[3] Y.Q. Song, X. Tang, One-shot method for measurement of diffusion, J. Magn. Reson. 170 (2004) 136–148.
[4] J.P. Stamps, B. Ottink, J.M. Visser, J.P.M. van Duynhoven, R. Hulst, A novel approach to a true spectroscopic single-scan diffusion measurement, J. Magn. Reson. 151 (2001) 28–31.
[5] G. Pages, P.W. Kuchel, NMR methods for fast recording of diffusion, in: S. Brandani, C. Chmelik, J. Kärger, R. Volpe (Eds.), Diffusion Fundamentals II, Leipziger Universitätsverlag, Leipzig, 2007, pp. 52–68.
[6] E.O. Stejskal, J.E. Tanner, Spin diffusion measurements: spin echoes in the presence of a time-dependent field gradient, J. Chem. Phys. 42 (1965) 288–292.
[7] C. Buckley, K.G. Hollingsworth, A.J. Sederman, D.J. Holland, M.L. Johns, L.F. Gladden, Applications of fast diffusion measurement using Difftrain, J. Magn. Reson. 161 (2003) 112–117.
[8] G. Bodenhausen, R. Freeman, G.A. Morris, Simple pulse sequence for selective excitation in Fourier-transform NMR, J. Magn. Reson. 23 (1976) 171–175.
[9] G.A. Morris, R. Freeman, Selective excitation in Fourier-transform nuclear magnetic-resonance, J. Magn. Reson. 29 (1978) 433–462.
[10] J. Hennig, Multiecho imaging sequences with low refocusing flip angles, J. Magn. Reson. 78 (1988) 397–407.
[11] A. Sodickson, D.G. Cory, A generalized *k*-space formalism for treating the spatial aspects of a variety of NMR experiments, Prog. Nuclear Magn. Reson. Spec. 33 (1998) 77–108.
[12] T.J. Mosher, M.B. Smith, A Dante tagging sequence for the evaluation of translational sample motion, Magn. Reson. Med. 15 (1990) 334–339.
[13] S. Peled, C.H. Tseng, A.A. Sodickson, R.W. Mair, R.L. Walsworth, D.G. Cory, Single-shot diffusion measurement in laser-polarized gas, J. Magn. Reson. 140 (1999) 320–324.
[14] L. Zha, I.J. Lowe, Optimized Ultra-fast Imaging Sequence (OUFIS), Magn. Reson. Med. 33 (1995) 377–395.
[15] T.R. Saarinen, C.S. Johnson, Imaging of transient magnetization gratings in NMR—analogies with laser-induced gratings and applications to diffusion and flow, J. Magn. Reson. 78 (1988) 257–270.
[16] D. Canet, J. Brondeau, C. Roumestand, Analytical expressions for the Dante pulse sequence, J. Magn. Reson. A 117 (1995) 103–108.
[17] P.V. Yushmanov, I. Furó, A rapid-mixing design for conventional NMR probes, J. Magn. Reson. 175 (2005) 264–270.
[18] P.V. Yushmanov, I. Furó, P. Stilbs, Micellar kinetics of a fluorosurfactant through stopped-flow NMR, Langmuir 22 (2006) 2002–2004.